2014

Post Eruption inflation of the East Pacific Rise at 9°50' N

Scott L. Nooner

Spahr C. Webb

W. Roger Buck

Marie-Helene Cormier
University of Rhode Island, milenecormier2@gmail.com

Citation/Publisher Attribution

Nooner, S. L., S. C. Webb, W. R. Buck, and M.-H. Cormier (2014), Post Eruption inflation of the East Pacific Rise at 9°50' N, *Geochem. Geophys. Geosyst.*, 15, 2676–2688, doi: 10.1002/2014GC005389.
Available at: https://doi.org/10.1002/2014GC005389

AGU PUBLICATIONS

Geochemistry, Geophysics, Geosystems

RESEARCH ARTICLE

10.1002/2014GC005389

Key Points:
- Volcanic inflation is occurring near 9°50′ N on the East Pacific Rise
- This is the first record of volcanic inflation at a normal mid-ocean ridge

Correspondence to:
S. L. Nooner,
nooners@uncw.edu

Citation:
Nooner, S. L., S. C. Webb, W. R. Buck, and M.-H. Cormier (2014), Post Eruption inflation of the East Pacific Rise at 9°50′ N, *Geochem. Geophys. Geosyst.*, *15*, 2676–2688, doi:10.1002/2014GC005389.

Received 18 APR 2014
Accepted 2 JUN 2014
Accepted article online 6 JUN 2014
Published online 30 JUN 2014

Post Eruption inflation of the East Pacific Rise at 9°50′ N

Scott L. Nooner[1], Spahr C. Webb[2], W. Roger Buck[2], and Marie-Helene Cormier[3]

[1]Department of Geography and Geology, University of North Carolina Wilmington, Wilmington, North Carolina, [2]Lamont-Doherty Earth Observatory, Columbia University, Palisades, New York, [3]University of Rhode Island, Graduate School of Oceanography, Narragansett, Rhode Island

Abstract In June 2008, we installed a geodetic network at 9°50′ N on the East Pacific Rise to track the long-term movement of magma following the 2005/6 eruption. This network consists of 10 concrete benchmarks stretching from the ridge to 9 km off-axis. During three campaign-style surveys, measurements of vertical seafloor motions were made at each of these benchmarks by precisely recording ambient seawater pressure as a proxy for seafloor depth with a mobile pressure recorder (MPR). The MPR was deployed using the manned submersible *Alvin* in 2008 and 2009 and the remotely operated vehicle *Jason* in 2011. The MPR observations are supplemented with data from a multiyear deployment of continuously recording bottom pressure recorders (BPRs) extending along this segment of the ridge that can record rapid changes in seafloor depth from seafloor eruptions and/or dike intrusions. These measurements show no diking events and up to 12 cm of volcanic inflation that occurred from December 2009 to October 2011 in the area of the 2005/6 eruption. These observations are fit with an inflating point source at a depth of 2.7 km and volume change of 2.3×10^6 m^3/yr located on the ridge axis at approximately 9°51.166′ N, 407 m from our northernmost benchmark, suggesting that the magma chamber underlying this segment of the ridge is being recharged from a deeper source at a rate that is about half the long-term inflation rate observed at Axial Seamount on the Juan de Fuca Ridge. These data represent the second location that active volcanic uplift has been measured on a mid-ocean ridge segment, and the first on a nonhotspot influenced segment.

1. Introduction

The East Pacific Rise (EPR) at 9°50′N is a fast spreading mid-ocean ridge (MOR) separating the Pacific and Cocos plates (Figure 1) which move away from each other at a full rate of about 110 mm/yr [*Carbotte and McDonald*, 1992] while the entire ridge system migrates to the north-west at 50 mm/yr relative to a hotspot reference frame [*Gripp and Gordon*, 2002]. It is one of the best-studied MOR segments in the world and it supports a dynamic hydrothermal system fueled by repeated dike intrusions and eruptions. The first documented eruption occurred in 1991/1992 [*Haymon et al*., 1993; *Rubin et al*., 1994], and since that time scientists have regularly returned to document changes in ecosystem, vent-fluid chemistry, and temperature, and to conduct detailed geological mapping. Because of these studies, when another eruption occurred in 2005/2006 [e.g., *Fornari et al*., 2012; *Tolstoy et al*., 2006], seismicity changes associated with the event were recorded on a local array of Ocean Bottom Seismometers (OBSs). Using a submersible, *Soule et al*. [2007] mapped out the extent of new lava flows in a 17 km long region of the EPR (Figure 1).

These eruptive events drive changes in the composition of vent fluids [*Fornari et al*., 2012; *Von Damm*, 2004, p. 2013; *Yücel and Luther*, 2013] and affect the temporal succession of biological communities surrounding the vents [*Luther et al*., 2012; *Shank et al*., 1998]. Between these diking events, magma is presumably redistributed subsurface and the underlying magma lens may be refilled, causing changes in depth of the seafloor above, a behavior that has previously been measured only at Axial Seamount on the Juan de Fuca Ridge [*Chadwick et al*., 2012, 2006; *Nooner and Chadwick*, 2009]. The presence of a shallow axial magma body a few tens of meters thick and 0.5-4.5 km wide within the EPR was first established from a multichannel seismic (MCS) experiment in 1985 [*Detrick et al*., 1987; *Kent et al*., 1993a, 1993b; *Vera et al*., 1990]. 3-D MCS data acquired in 2008 extend the earlier observations and have allowed fine-scale details regarding crustal magma distribution to be revealed [*Carbotte et al*., 2012]. Magma lens segments 5–20 km in length are present along axis, with many segment ends corresponding to discontinuities in seafloor structures [*Carbotte et al*., 2013].

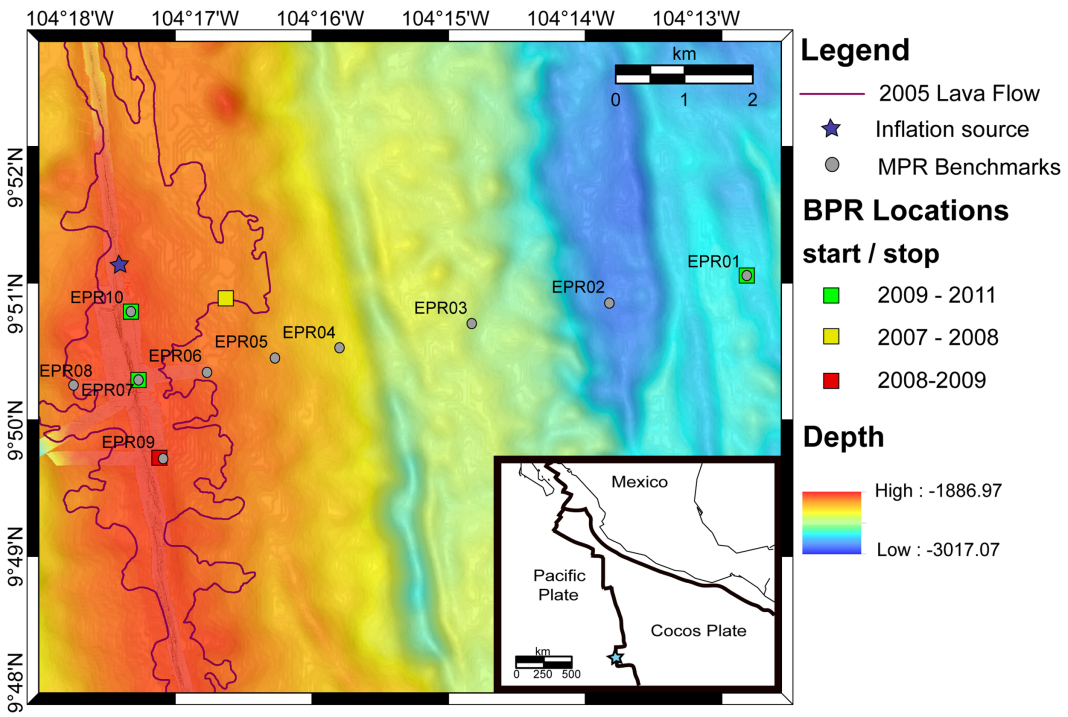

Figure 1. Bathymetry map of the study area is shown with locations of seafloor benchmarks (gray circles), BPR deployment locations (squares), and the location of the best-fitting inflation source (dark blue star). Benchmarks EPR09, EPR07, and EPR10 are located just east of the ridge axis, less than 100 m from the Axial Summit Trough (AST). The outline from the 2005–2006 eruption [*Soule et al.*, 2007] is indicated by the purple line.

In this paper, we present results from a series of three geodetic surveys that were carried out at 9°50′N on the EPR using water pressure measurements on top of a network of 10 concrete benchmarks that were emplaced on the seafloor in June 2008 (Figure 1). Our results allow us to compare magma recharge at the fast spreading EPR with the hot-spot influenced intermediate spreading rate Axial Seamount segment of the Juan de Fuca ridge—the only other submarine mid-ocean ridge site with documented magmatic uplift. We also compare results with observations made on recently-active, subaerial spreading centers in Iceland and Ethiopia which are also hotspot influenced. Eruptions have been geodetically detected as sudden deepening of the surface of the crust over magma chambers on Axial Volcano [*Chadwick et al.*, 2006, 2012; *Fox*, 1999; *Nooner and Chadwick*, 2009], in Iceland [*Einarsson*, 1991], and most recently the Afar of Ethiopia [e.g., *Ayele et al.*, 2007]. In Iceland and Ethiopia dike intrusion, events producing meter-scale graben subsidence also produce tens of centimeter flanking uplift, while other dike events produce only uplift [e.g., *Wright et al.*, 2012]. Post eruption deformation at these locations has been observed and interpreted as due to either magma recharge or viscoelastic relaxation [e.g. *Nooner and Chadwick*, 2009; *Nooner et al.*, 2009].

The implementation of geodetic monitoring experiments in the marine environment has been a challenge. Seafloor geodetic techniques include acoustic ranging between pairs of instruments such as extensometers [*Chadwell et al.*, 1999; *Chadwick and Stapp*, 2002; *Chadwick et al.*, 1999; *McGuire and Collins*, 2013; *Nagaya et al.*, 1999], combined GPS/acoustic positioning of instruments on the bottom from surface ships [e.g., *Chadwell et al.*, 1995; *Fujimoto et al.*, 1998; *Fujita et al.*, 2003; *Gagnon et al.*, 2005; *Ito et al.*, 2011; *Osada et al.*, 2003; *Sato et al.*, 2011; *Spiess et al.*, 1998], long and short baseline tiltmeters [*Anderson et al.*, 1997; *Tolstoy et al.*, 1998], and seafloor gravity measurements [e.g., *Ballu et al.*,1999, 2009, 1998; *Nooner et al.*, 2007; *Sasagawa et al.*, 2003]. Although each of these techniques has advantages, one of the simplest and most successful techniques has been the combined use of bottom pressure recorders (BPRs) and mobile pressure recorders (MPRs). BPRs sit on the seafloor and continuously record ambient pressure as a proxy for seafloor depth [*Fox*, 1999; *Fujimoto et al.*, 2003; *Watanabe et al.*, 2004] using sea level as a datum so that any uplift or subsidence of the seafloor causes a corresponding decrease or increase in measured pressure. The BPRs we used in this study were built at Lamont-Doherty Earth Observatory and use Paroscientific Digiquartz model

Table 1. BPR Deployment Locations

Benchmark	Latitude (N)	Longitude (W)	Deployment Dates
BPR08	9.85057	104.27936	Feb 2007 to Jun 2008
BPR08	9.82967	104.28835	Jun 2008 to Dec 2009
BPR08	9.84007	104.29063	Dec 2009 to Oct 2011
BPR01	9.84880	104.29210	Dec 2009 to Oct 2012
BPR06	9.85338	104.20995	Dec 2009 to Oct 2013

410K pressure transducers. These gauges are subject to long-term linear drift in pressure of up to 150 ppm that can yield inferred height changes up to 38 cm/yr at a depth of 2500 meters, the depth of the axial summit trough (AST) [*Chadwick et al*., 2006; *Fujimoto et al*., 2003; *Polster et al*., 2009; *Watts and Kontoyiannis*, 1990]. The exact rate of drift is specific to each sensor and stabilizes during the first few weeks of deployment while the sensor equilibrates [*Eble et al*., 1989; *Fox*, 1990]. Because of the inherent drift, these instruments are very good for observing sudden, short period, or episodic events, but are inadequate for observing long-term or gradual deformation.

Campaign style measurement using MPRs [*Chadwick et al*., 2012, 2006; *Nooner and Chadwick*, 2009; *Sasagawa et al*., 2003; *Stenvold et al*., 2006] are analogous to optical leveling on land, but involve making pressure measurements on an array of fixed seafloor benchmarks. The MPR instrument consists of two Paroscientific Digiquartz pressure transducers (again, model 410K in this study). The advantage of this technique is that the drift in the pressure gauges can be calculated by assuming no relative deformation occurs during the survey (typically 2–3 days). The disadvantage of this technique is that all the measurements are made with respect to a reference benchmark, which is assumed to be stationary over time. This requires a site outside of the region of expected deformation. MPR uncertainties are typically less than 0.9 cm [*Chadwick et al*., 2012, 2006; *Nooner and Chadwick*, 2009] and have been as low at 0.5 cm [*Nooner et al*., 2007; *Stenvold et al*., 2006]. BPRs and MPR measurements are typically colocated to allow drift calibration of the BPRs.

Here we present results from BPR records and three MPR surveys at 9°50′N on the EPR, spanning 3.5 years, that show uplift occurring subsequent to the 2005–2006 eruption. We use the deformation to estimate the location of the inflation source and the magma supply rates and compare to what has been observed at Axial Seamount on the Juan de Fuca Ridge, Iceland and Ethiopia.

2. Methods and Results

A bottom pressure recorder (BPR08) was deployed near the 9°50′ N AST beginning in 2007. BPR08 was then recovered, serviced, and redeployed in both 2008 and 2009, colocated with MPR benchmarks EPR09 and EPR07, respectively. BPR08 stopped working shortly after being redeployed in 2009. Additional BPRs were deployed in 2009; BPR01 was deployed at benchmark EPR10 and BPR06 was deployed at benchmark EPR01 (Figure 1 and Table 1).

The BPRs collected data at a 40 Hz sample rate. The data were filtered to remove the variation in pressure caused by the ocean tides. Records were converted to depth using the standard ocean depth formula derived by *Fofonoff and Millard* [1983]. A detailed discussion of this procedure is given in *Nooner* [2005]. The resulting BPR records shown in Figure 2 are difficult to interpret because of gauge drift that varies from instrument to instrument and large (order 20cm) pressure signals of oceanographic origin. The oceanographic signals can be mostly removed by differencing adjacent sites (not shown), but the unpredictable gauge drift limits the usefulness of the BPR data for assessing slow geodetic changes. Instrument drift in BPR06 (order 1m) is clearly evident (Figure 2d) as it is unlikely to have experienced any uplift at all since it is colocated with the reference benchmark, EPR01, ~9 km from the AST. This illustrates the importance of combining BPR and MPR measurements in seafloor geodetic studies like this one.

Eruptions have been observed to produce large (order 1m) drops in seafloor elevation over time intervals of only a few hours as the underlying magma chamber deflates during the eruption [*Chadwick et al*., 2012, 1999; *Nooner and Chadwick*, 2009] and similar drops are seen over magma chambers during dike propagation events in Iceland [e.g. *Einarsson*, 1991]. We see no such events in the BPR data suggesting no eruption

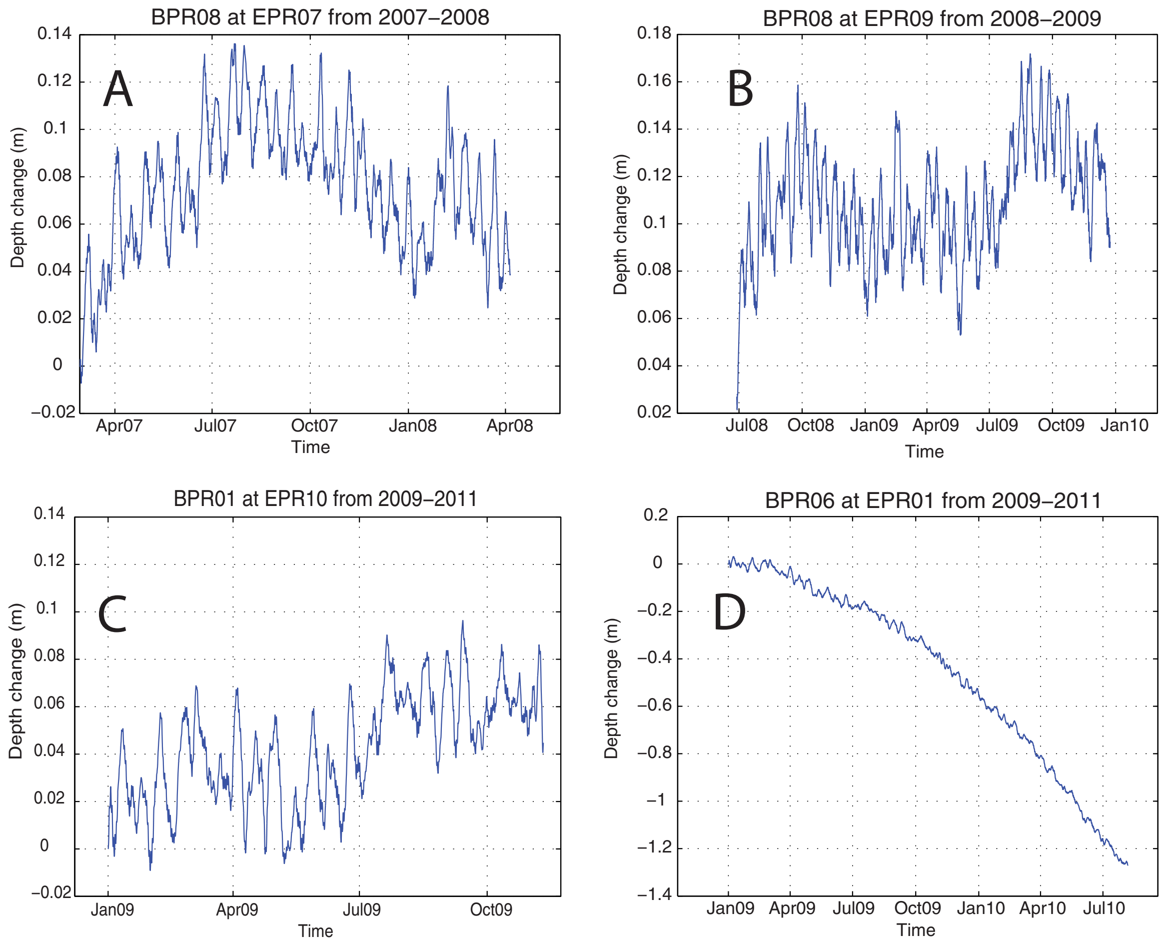

Figure 2. Filtered BPR data from at the study site showing (a) BPR08 at site EPR07 from March 2007 to April 2008, (b) BPR08 at site EPR09 from July 2008 through December 2009, (c) BPR01 at EPR10 from January 2009 to December 2009, and (d) BPR06 at site EPR01 from January 2009 to August 2010. The BPR pressure data have been converted to depth and tidal frequencies have been filtered out using a low-pass Butterworth filter.

or dike events occurred from March 2007 until at least November 2010 in the vicinity of the instruments. Over this short-timescale, drift of the gauges and oceanographic signals (other than the tide signal which can be removed) produce negligible change in pressure and thus we can conclude that no rapid elevation changes with amplitudes more than a few centimeter have occurred during the observation interval. The batteries died in BPR01 and BPR06 before we recovered the instruments in October, 2011.

BPR observations at one additional site about 30km to the north (10°04.7282′N, 104°20.2179′W), and three sites at about 27km (9°35.0257′N, 104°15.3048′W), 35km (9°30.3978′N, 104°14.7812′W), and 56km (9°19.0′N, 104°13.0′W) south of the benchmarks also show no evidence for rapid vertical elevation changes that would be indicative of eruptions elsewhere on this ridge segment. These data extend from May 2007 until about mid October 2011.

MPR surveys were carried out during research cruises on board the *RV Atlantis* in June 2008, December 2009, and October 2011. Before MPR measurements were made in 2008, 10 concrete benchmarks (Figure 3) weighing approximately 91 kg in water were installed on the seafloor. The benchmarks span a range of distances from the AST in order to allow any observed displacement to be compared to deformation models. Benchmark names and locations are shown in Figure 1 and site characteristics are given in Table 2. The benchmarks far from the AST were located on a layer of pelagic sediments that increased in thickness with distance from the AST. The benchmarks legs were pushed completely into the mud (Figure 3a) using the hydraulic manipulator arm of the HOV *Alvin* during installation. The first two surveys were conducted using the manned DSV *Alvin* and the final survey was conducted using the ROV *Jason*. Although it was not our

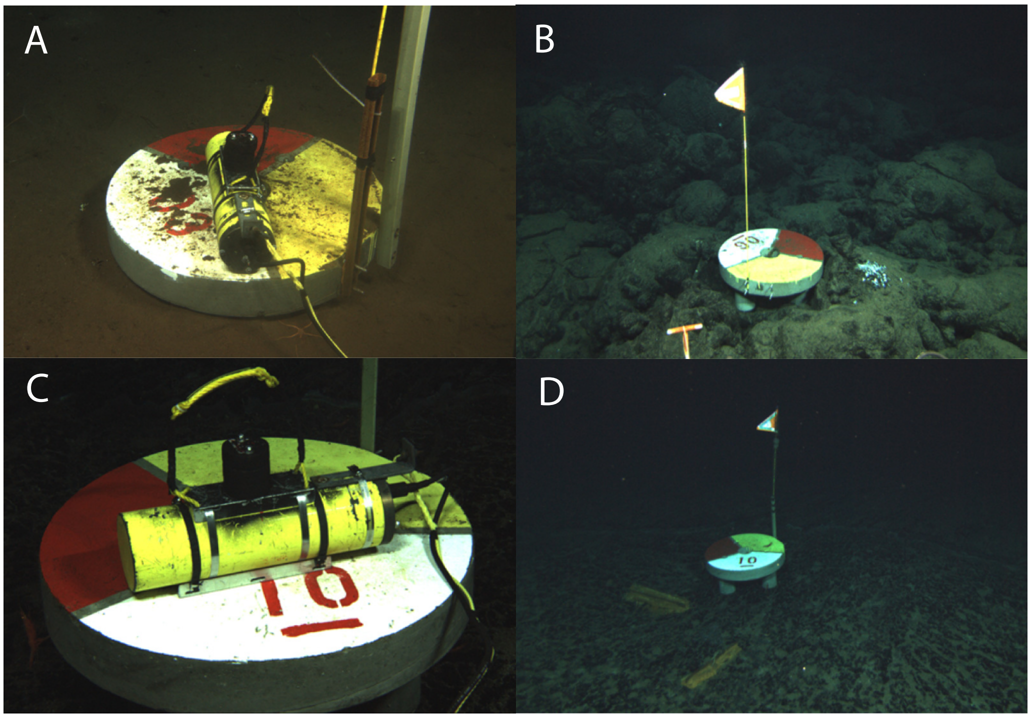

Figure 3. Concrete seafloor benchmarks are shown for three locations in the survey area representative of the types of terrain at the study site. (a) EPR03 is shown with its tripod legs buried in the thick off-axis sediments. (b) EPR06 is shown on top of and surrounded by pillow basalts. (c) Close up of the MPR instrument package making a measurement on top of benchmark EPR10. (d) EPR10 is shown on top of sheet flows emplaced during the 2005–2006 eruption.

original intent, the use of the HOV *Alvin* rather than the ROV *Jason* meant the first two surveys became a test of our MPR instrument limitations and survey techniques, and as such provided us with valuable lessons on survey design and instrument limitations, as described in the next section.

The MPR pressure data were reduced by first removing the effect of tides and then calculating and removing instrument drift. Continuous BPR data collected at the AST (Figure 2, shown with tides removed) were used to correct the MPR data for ocean tides in years 2007 and 2009. The BPRs were no longer recording during the 2011 survey, so the SPOTL tide model was used to make ocean tide corrections [*Agnew*, 1997]. The BPR data showed good agreement with the SPOTL model in the first two surveys. Following the methods described in *Chadwick et al*. [2006] and *Nooner* [2005], the linear drift of the MPR instrument was determined each year from repeated measurements on each benchmark. After correcting for ocean tides and linear instrument drift, the pressure data were then converted to depth using the standard ocean depth formula derived by *Fofonoff and Millard* [1983]. The resulting uncertainty of the MPR measurements is given by the scatter of repeated measurement on

Table 2. MPR site Characteristics

	Benchmark Locations			Number of Measurements Each Year		
Benchmark	Lat. (N)	Lon. (W)	Depth (m)	2008	2009	2011
EPR01	9.85338	104.20995	2787	3	3	2
EPR02	9.85005	104.22802	2851	2	3	1
EPR03	9.84732	104.24635	2688	1	2	2
EPR04	9.84410	104.26388	2611	2	3	2
EPR05	9.84292	104.27290	2556	5	2	2
EPR06	9.84107	104.28167	2529	2	4	2
EPR07	9.84007	104.29063	2501	6	11	5
EPR08	9.83913	104.29970	2520	2	5	1
EPR09	9.82970	104.28795	2506	4	2	1
EPR10	9.84880	104.29211	2509	2	3	1

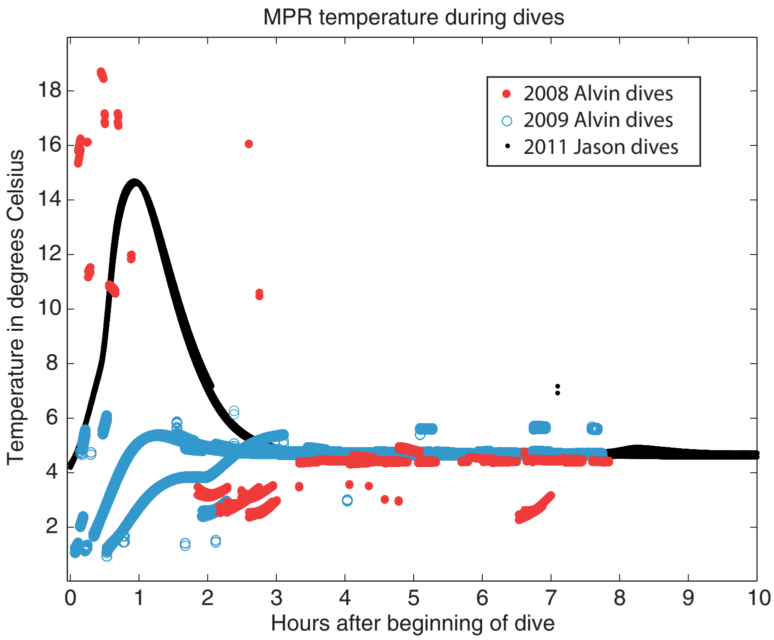

Figure 4. MPR Paroscientific 410K gauge temperature records are shown for all 2008 nine HOV *Alvin* dives (red-filled circles), all nine 2009 HOV *Alvin* dives (blue-unfilled circles), and the first 10 h of the two ROV *Jason* dives in 2011 (small black-filled circles). The temperature changes rapidly following the start of the dives in each year, but the temperature range and dive to dive scatter is the greatest in 2008. The extremely low temperatures seen in some 2008 measurements are from cooling of the instrument when powered off for transits. As a result, power to the MPR was maintained for 2009 and 2011. By using an ice-box (see text) for launch in 2009, temperature variations during each dive were greatly reduced.

all the benchmarks for each survey and is 3.5, 2.2, and 0.6 cm in 2008, 2009, and 2011, respectively (Table 3; all uncertainties given are one σ). Our results in 2008 are 7 times worse than the results from *Stenvold et al*. [2006] and more than 3–4 times worse than recent results from Axial Seamount [*Chadwick et al*., 2012, 2006; *Nooner and Chadwick*, 2009], due to temperature changes in the instrument that occurred during each short HOV *Alvin* dive and drift correction errors. This is discussed in more detail in a later section. Our results in 2011, however, are as good or better than measurements that have made anywhere else, indicating that high-quality data are achievable at the EPR. In the following three sections, we discuss each of the three surveys in detail.

2.1. Survey One

Although Paroscientific 410K pressure gauges are temperature compensated, rapid changes in temperature have been shown to impact their pressure output value [e.g. *Nooner*, 2005]—there can be a time lag between the change in temperature of the gauge and the correction made for temperature change. For example, *Chadwick et al*. [2006] found that it took $\sim$2 h for the pressure gauges to equilibrate once on bottom at Axial Seamount. Previous surveys in the North Sea, however, were able to achieve 0.5 mm measurement repeatability without waiting additional time on bottom [*Sasagawa et al*., 2003; *Stenvold et al*., 2006]. In fact, in these North Sea surveys the ROV was usually recovered to deck and the instruments were placed in a bath of temperature-controlled ice water before transiting to the next benchmark. This method was efficient because the water depth ranged only from 80 to 300 m, and launches and recoveries of the ROVs took little time ($\sim$10 min). Because of this previous work, we were hopeful that similar results could be obtained in the deeper water over the EPR using the DSV *Alvin*.

During our survey, the MPR instrument was kept in an ice bath while on deck. It was taken out of the ice bath just prior to launch and was put back into the ice bath immediately following vehicle recovery, following the procedure of *Sasagawa et al*. [2003] and *Stenvold et al*. [2006]. Unfortunately, we underestimated (1) the time *Alvin* would spend in the warm surface waters of the EPR and (2) how rapidly the MPR would warm up, even after spending >12 hours in an ice bath. Each *Alvin* dive in 2008 took the MPR from an internal temperature of almost 19°C to bottom temperatures as low as 2°C and back during an 8 h period (Figure 4). The short periods of temperatures approaching 2°C that can be seen in Figure 4 result from power being turned off to the MPR instrument during transits. There is a small offset in the location of the temperature sensor and the pressure oscillator within the Paroscientific transducers, resulting in poor temperature corrections during periods of rapid temperature changes (this is discussed in more detail below). By comparison, internal temperature changes during similar surveys in the North Sea were only a few degrees

Celsius [*Stenvold et al*., 2006]. We attribute our observed uncertainties of 3.5 cm (T3) to the large and rapid temperature fluctuation the MPR experienced and to poor drift corrections. This level of uncertainty is much higher than we expected based on previous studies. The drift correction uncertainties were high because attempts to complete each dive as a closed loop were not possible given the station spacing and limited bottom time of the DSV *Alvin*, particularly in the 2008 survey. Most of the nine *Alvin* dives were shared with another investigator, making it even more difficult to complete a closed loop survey during most dives, and providing another reason that the MPR was periodically powered down. During off axis dives with long transits, we typically ran out of time or battery power in the submersible before being able to complete a loop. Attempts to develop a temperature correction curve did not reduce the repeatability of the overall survey.

2.2. Survey Two

The second survey was carried out in December, 2009. Because of our results from the first survey, we were scheduled to use the ROV *Jason* for the second survey but logistical problems forced us to use the DSV *Alvin* again on short notice. We used three strategies to improve our results over the first survey: (1) We carefully planned each dive to optimize the number of repeats during the dive. This allowed us to more accurately estimate a temperature correction curve that we could apply to each dive. (2) We mounted an ice-filled box to the basket of the DSV *Alvin* to contain the MPR during the dive descent. This isolated the gauges from warming in the surface water prior to descent, thereby minimizing the temperature fluctuations between the ice bath on the deck of the ship and the 2° C bottom waters of the EPR (Figure 4). (3) The last major strategy to improve data quality was that in addition to our normal MPR, attached via cable to the vehicle, we deployed a small battery powered MPR on the last benchmark of each dive. We then started the next dive at that benchmark. This alternate MPR was meant to be the reference gauge that maintained a stable temperature throughout the duration of the survey. This was an instrument that we put together in the week prior to the cruise from spare parts and an unused pressure case that we repurposed. Although it passed the *Alvin* certification procedure prior to the cruise, the pressure case flooded a few days into the survey and no data were recovered.

The resulting 2009 benchmark height uncertainties are estimated to be 2.2 cm (Table 3). This is better than the previous survey, due primarily to the addition of the ice-filled box on the front basket of *Alvin* that the MPR was kept in during submersible deployment and descent. We were also able to plan more dives that contained repeated measurements, allowing us to better determine the instrument drift. The single dive repeatability in 2009 was 0.9 cm based on the final dive, which had five repeats, showing that it is possible to carry out a high-quality survey using Alvin with proper station spacing. A linear correction taken from this dive was used to correct the other dives for temperature.

2.3. Survey Three

The ROV *Jason* was used for the final survey, which took place in October, 2011. In spite of a hurricane, a broken Jason/Medea tether, and a winch failure (all of which consumed considerable ship time and significantly decreased the number of measurements we were able to make) we achieved excellent results (Table 3) with a repeatability of 0.6 cm during two dives. It must be noted that although benchmarks 2, 8, 9, and 10 received only one visit in 2011, benchmark 7 received five visits and all others received two visits each. Uncertainties were calculated based on the repeats of these six stations (Table 2). Temperature records are shown as black circles in Figure 4.

Table 3. Error Budget

	Depth Uncertainty (cm)		
Error Source	2008	2009	2011
Inherent precision of pressure sensor	0.1	0.1	0.1
Background noise	0.4	0.4	0.4
Calibration uncertainty	0.3	0.3	0.3
Tide correction uncertainty	0.5	0.5	0.5
Drift correction	1.5	0.8	0.3
Depth conversion	0.5	0.5	0.5
Rotational uncertainty	0.1	0.1	0.1
Temperature uncertainty	3.0	2.0	0.1
Root sum of squared errors (expected repeatability)	3.5	2.4	0.9
Observed repeatability	**3.5**	**2.2**	**0.6**

2.4. Temperature Corrections

Pressure is measured within the Paroscientific 410K pressure transducers by utilizing an oscillating quartz crystal beam than is mechanically connected to a C-shaped Bourdon tube (http://www.paroscientific.com). Changes in fluid pressures within the Bourdon tube and temperature changes of the quartz beam result in changes in the oscillation frequency of the quartz beam. Since we are only interested in measuring changes in pressure, a temperature correction must be made. To make this correction, temperature within the transducers is measured using a quartz crystal torsional tuning fork temperature sensor (http://www.paroscientific.com). Since the quartz beam and the torsional tuning fork cannot be located in the exact same place, the temperature being measured is at a slightly different location than the quartz beam.

There are two sources of error resulting from the corrections described above: (1) Due to the small offset between temperature sensor and pressure sensor, temperature gradients can cause the temperature and pressure sensors to experience different temperatures. Due to the thermal mass of the instrument, large changes in temperature, like what we observe from the ocean surface to the seafloor, take some time to fully equilibrate. The larger the temperature change is, the longer the equilibration time. While the instrument is equilibrating, there is a changing temperature gradient that can affect the pressure output. (2) Changes in gauge temperature most likely result in a change in the shape of the Bourdon tube itself due to thermal expansion or contraction. This results in small differences in the apparent pressure.

The temperature records for the three surveys shown in Figure 4 show a similar broad-scale trends. In general, the MPR instrument begins a dive cool (since it was kept in a bucket of ice water prior to the dives), then goes through a period of rapid warm-up once contact is made with the ocean surface waters. This is followed by a period of rapid cool down as the outside water temperature decreases with depth, and finally a period of relatively stable temperatures. The *Jason* dives show a much more repeatable temperature profile than the *Alvin* dives do, which show particularly large variability in 2008 before we used an ice-box on the science basket to carry down the MPR. The temperature of the instrument during the *Jason* dives stabilizes after about 3 h (it takes about 1.5 h to reach the bottom) with very few fluctuations for the rest of the dive (only the first 10 h of each dive are shown). The temperature of the instrument during the *Alvin* dives is similar, but with much more variability. Part of this variability in gauge temperature is due to MPR power being turned off to conserve power during *Alvin* transits. In retrospect, this was not good practice since loss of power to the MPR allowed the instrument to cool down by almost 2°C. Power was restored to make the subsequent measurement, causing the MPR electronics to heat the interior of the instrument and inducing a temperature gradient in the pressure transducers. Aside from a single dive, the MPR power was kept on for the duration of each dive during the 2009 survey.

The Paroscientific 410K pressure transducers we used in these surveys have temperature corrections factors that range from 20 to 120 cm/°C at the survey depths. The following exercise illustrates the magnitude of the errors we might expect from turning the MPR power off during transits, as was done in much of the 2008 survey. The pressure transducers are enclosed inside a cylindrical aluminum pressure case (Figure 3) that is about 16 cm in diameter. If we assume that the aluminum walls are at 2°C and the MPR electronics are at 4°C, then a rough estimate of the temperature gradient from the center to the walls of the MPR is 0.25°C/cm. Therefore, if the torsional tuning fork is 0.1 cm from the quartz beam (this is an estimate only), we would expect that the temperature difference between the two locations would be about 0.025°C. The resulting temperature correction translates to depths errors ranging from 0.5 to 3 cm, depending on the gauge.

The very small temperature uncertainty for 2011 (Table 3) results from the fact that the majority of the measurements during the two ~24 h *Jason* dives were made significantly after the 3 h equilibration time after the dives began and there were only two dives. In addition to the temperature correction errors discussed above, the 2008 and 2009 surveys were both carried out over the course of nine *Alvin* dives, during which at least 1/4 of the measurements were made before the gauges had equilibrated.

3. Discussion

Figure 5 shows the benchmark heights each year relative to the reference benchmark EPR01. The uncertainty in benchmark height changes from 2008 to 2009 is 4.1 cm—the square root of the sum of the squared uncertainties for each year. Within this uncertainty, we cannot be confident of any benchmark height changes during that time. However, this null result puts an upper bound of about 8.1 cm on the

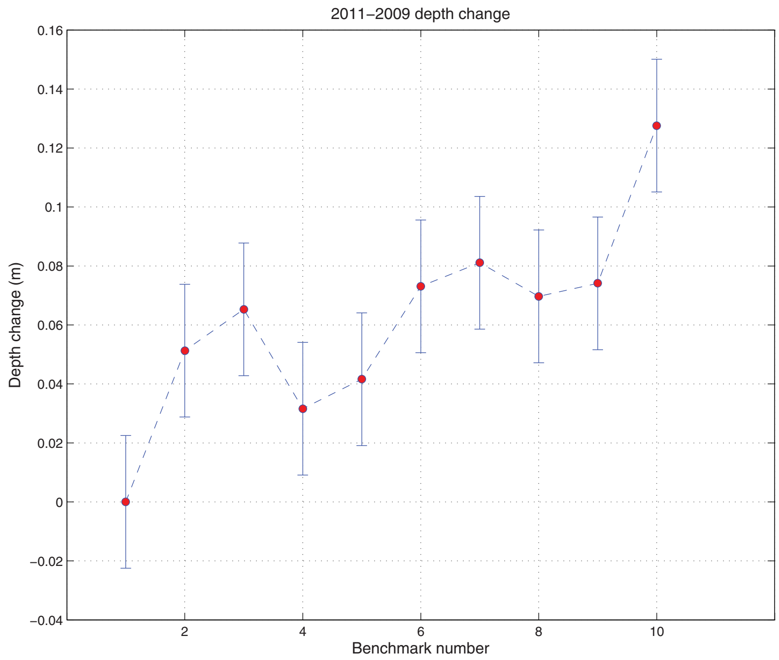

Figure 5. Benchmark depth changes from 2009 to 2011 are shown along with measurement uncertainties (1 σ).

maximum deformation that could have occurred at 9°50′ N during that time window. From December 2009 to October 2011, we observe up to 12 cm of uplift on benchmark EPR10 (Figure 5). This exceeds the combined 2.3 cm uncertainty for the 2008–2009 time span by a factor of 5, giving us confidence in our observations. Uplift generally decreases with distance from EPR10 (Figures 5 and 6), suggesting that the deformation results from volcanic inflation at the AST, however, benchmarks EPR02 and EPR03 show anomalous uplift compared to this trend. This may be caused by tectonics (i.e., faulting) but is more likely due to either measurement errors in 2008 or benchmark instabilities.

We fit the observed deformation from 2009 to 2011 using a point source inflation model [*Mogi*, 1958] with a Poisson's ratio of $\upsilon = 0.296$, which we calculated from Vp/Vs ratios that have been measured for depths of 1–3 km at this location [e.g., *Vera et al*., 1990; *Waldhauser and Tolstoy*, 2011]. Decreasing Poisson's ratio decreases the volume change of the optimum inflation source, while the depth remains the same. If we remove the results from benchmarks EPR02 and EPR03, the deformation data can be fit with a point source located on the ridge axis 407 m northeast of our benchmark EPR10 (best fit is at 9°51.166′N and 104°17.540′ W; Figures 1 and 6). This location roughly coincides with a fourth-order discontinuity in the ridge morphology and the boundary between two seismically imaged shallow axial melt lens segments from *Carbotte et al*. [2013]. The best fitting point source depth is 2.7 km, whereas the magma lenses from *Carbotte et al*. [2013] lie at about 1.5 km depth at this location. Interestingly, *Marjanovic* [2013] and *Marjanovic et al*. [2013] found a region of enhanced melt underlying the melt lens over most of this segment of the EPR, except in the location of our best fitting inflation source. They showed that melt present in the midcrust underlying this region of the EPR from 9°50′ to 9°52′ N is

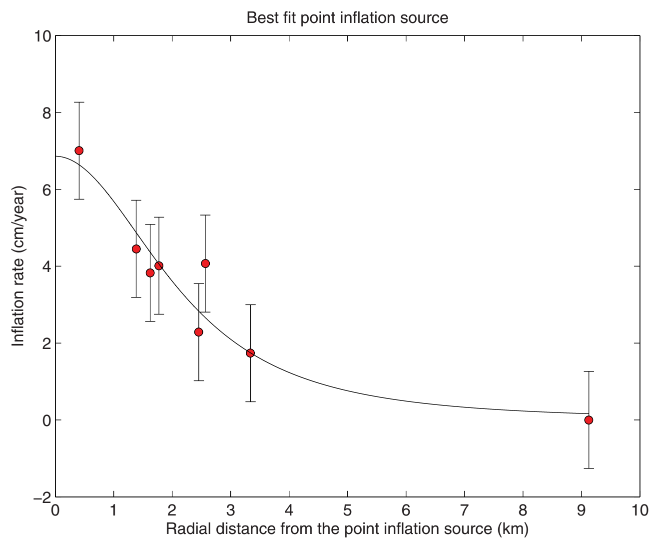

Figure 6. The best fitting point inflation source [*Mogi*, 1958] is shown (black line) along with inferred inflation rates calculated from benchmark depth changes from 2009 to 2011. Uncertainties shown are 1 σ. The location of the inflation source is shown in Figure 1 and the depth is 2.7 km.

significantly lower than adjacent segments. Bathymetric and geochemical data [*Goss et al*., 2010; *Soule et al*., 2007; *White et al*., 2006] indicate that the source of the eruption was 9°48′ - 9°52′ N. *Marjanovic et al*. [2013] suggested that the 2005–2006 eruption was sourced initially from the midcrustal melt body 9°50′–9°52′ N, depleting the midcrust of melt in this region. Our geodetic results suggest that inflation could be occurring at a depth of about 2.7 km underlying the 9°51′ N region, consistent with a model of reinflation for a midcrustal magma region that drained due to the eruption. It is important to point out that a similar deformation pattern could be obtained for a shallower axisymmetric oblate spheroidal inflation source (a penny-shaped crack) if the ratio of radius to depth is greater than about 0.8 [*Fialko et al*., 2001]. This would mean that a 1.5 km deep penny-shaped magma chamber would have to be around 3 km wide; however, this analysis does not reflect the along-axis dimension of the observed magma lens [*Carbotte et al*., 2013].

Our results suggest that magmatic reinflation is occurring at 9°50′ N at a rate of 7 cm/yr, equivalent to a point source volume change of 2.3×10^6 m^3/yr. This is about 1/3 the rate of long-term inflation observed at Axial Seamount [*Chadwick et al*., 2006; *Nooner and Chadwick*, 2009]. Axial Seamount is a large volcanic seamount associated with the Cobb hotspot, so its magma supply is likely enhanced relative to a normal fast spreading mid-ocean ridge segment like the EPR at 9°50′ N. Rapid reinflation periods following both the 1998 and 2011 eruptions of Axial Seamount have been attributed to viscoelastic relaxation and/or poroelastic behavior of the mush region underlying the magma chamber [*Chadwick et al*., 2013; *Nooner and Chadwick*, 2009]. This period of inflation was very brief, lasting only a few months. Therefore, we believe that since the EPR eruption occurred 3–4 years prior to the observed uplift shown here, this phase of inflation was already past. If the observed inflation rate at the EPR represents a steady linear long-term inflation, we expect the magma chamber to be fully reinflated and primed for an eruption by 2026, after an approximately 20 year interval. We obtain this result by using 47×10^6 m^3 as the total volume of magma evacuated from the magma chamber during the 2005/6 eruption from *Soule et al*. [2007], and assuming a continuous inflation rate of 2.3×10^6 m^3/yr. This estimate is in general agreement with the known recurrence interval of 13 years between the 1992 and the 2005/2006 eruptions. The volume of the 2005/2006 eruption is only 25–33% of the volume of the two eruptions observed at Axial Seamount. This EPR site has a much smaller magma chamber than Axial Seamount as inferred from seismic studies [e.g., *Detrick et al*., 1987; *Soule et al*., 2007; *West et al*., 2001].

The only other constraints on magmatic inflation along spreading segments come from recent observations at two subaerial regions. The estimated inflation rate at 9°50′ N on the EPR is about a factor of 3 lower than the average 20 cm/yr inflation rate at the center of the Krafla spreading segment in Iceland over a 10 year episode of activity that began in 1975 [e.g., *Tryggvason*, 1984]. However, there were 20 dike intrusion and/or extrusion events in that episode over that period on this slow spreading segment. Also, the time interval since the last episode on the Krafla segment occurred 250 years before the 1975 sequence [e.g., *Einarsson*, 1991]. The only other constraint on magmatic reinflation on a spreading center comes from an episode of 14 dike intrusion events on the Dabbahu spreading segment in the Afar of Ethiopia that began in 2005. Six years of InSAR observations there show about 20 cm/yr of uplift of the segment center which is comparable to the rate seen for Krafla [e.g., *Wright et al*., 2012].

Our experiences at the EPR suggest that it is possible to carry out an MPR survey using the DSV *Alvin*; however, certain special precautions must be made. (1) Stowing the MPR inside a sealed ice-box during vehicle launch greatly reduces the temperature changes that the MPR experiences. This leads directly to lower uncertainties during the short *Alvin* dives because it reduces the temperature correction lag and shortens the time for the MPR to equilibrate with the water temperature near the seafloor. (2) Stations should be arranged to allow at least one repeat measurement during each dive. This will allow a combined temperature and drift correction to be made for each dive separately, as required by our observation that this correction varies from dive to dive. (3) Finally, an autonomous pressure gauge package should be used as an additional MPR and left on the seafloor the duration of the survey to add redundancy. This gauge would then be left on the final benchmark at the end of each dive and picked up at the beginning of the subsequent dive. Data from this gauge would then be the same as a typical ROV-based MPR survey.

4. Conclusions

In spite of challenging circumstances during each cruise, resulting in data uncertainties much greater than we expected, we have strong evidence that up to 12 cm of inflation (7 cm/yr) occurred at 9°50′ N on the

EPR between December 2009 and October 2011. The focus of this inflation is 407 m NNE of EPR10, on the ridge axis at a depth of 2.7 km. This location and depth coincide with the location of a magmatically depleted midcrust region that *Marjanovic et al*. [2013] observed following the eruption. The magma supply rate required is about half what has been observed as the "steady state" magma supply rate at Axial Seamount on the Juan de Fuca Ridge, suggesting a less vigorous magma supply underlies this part of the EPR.

The eruption occurred in 2005/2006, but our first survey was not conducted until 2008, more than 2 years after the eruption. We hypothesize that the observed inflation rate of 7 cm/yr represents the "steady state" supply from a deeper melt reservoir. This hypothesis can be tested via additional pressure measurements on the geodetic network that we have established.

The BPR data suggest that no new eruptions have occurred in the vicinity of the 2005 eruption between March 2007 and October 2011, nor have eruptions or dike intrusions occurred elsewhere along this ridge segment within the vicinity of one BPR 30 km to the north of the eruption site, or near three BPRs 27 to 50 km south of the site.

Acknowledgments
We thank the crew of the R/V Atlantis for making our three cruises successful and productive. We thank the National Deep Submergence Facility for their outstanding work on these three cruises, especially the HOV Alvin and the ROV Jason pilots. We also thank two anonymous reviewers for improving this manuscript. The data from this paper are available from the Marine Geoscience Data System (http://www.marine-geo.org). This research was funded by the US National Science Foundation (OCE-064780; OCE-0426575).

References

Agnew, D. C. (1997), NLOADF: A program for computing ocean-tide loading, *J. Geophys. Res.*, *102*(B3), 5109, doi:10.1029/96JB03458.

Anderson, G., S. Constable, H. Staudigel, and F. K. Wyatt (1997), A seafloor long-baseline tiltmeter, *J. Geophys. Res.*, *102*, 20269–20285, doi:10.1029/97JB01586.

Ayele, A., E. Jacques, M. Kassim, T. Kidane, A. Omar, S. Tait, A. Nercessian, J.-B. de Chabalier, and G. King (2007), The volcano–seismic crisis in Afar, Ethiopia, starting September 2005, *Earth Planet. Sci. Lett.*, *255*, 177–187, doi:10.1016/j.epsl.2006.12.014.

Ballu, V. S., J. A. Hildebrand, and S. C. Webb (1998), Seafloor gravity evidence for hydrothermal alteration of the sediments in Middle Valley, Juan de Fuca Ridge, *Mar. Geol.*, *150*, 99–111, doi:10.1016/S0025-3227(98)00024-3.

Ballu, V., J. A. Hildebrand, and E. L. Canuteson (1999), The density structure associated with oceanic crustal rifting at the Hess Deep: A seafloor and sea-surface gravity study, *Earth Planet. Sci. Lett.*, *171*, 21–34, doi:10.1016/S0012–821X(99)00132-6.

Ballu, V., et al. (2009), A seafloor experiment to monitor vertical deformation at the Lucky Strike volcano, Mid-Atlantic Ridge, *J. Geod.*, *83*, 147–159, doi: 10.1007/s00190–008–0248–3.

Carbotte, S., J. P. Canales, M. Nedimović, H. Carton, and J. Mutter (2012), Recent seismic studies at the East Pacific Rise 8°20′–10°10′N and endeavour segment: Insights into mid-ocean ridge hydrothermal and Magmatic processes, *Oceanography*, *25*, 100–112, doi:10.5670/oceanog.2012.08.

Carbotte, S. M., and K. McDonald (1992), East Pacific Rise 8°–10°30′N: Evolution of ridge segments and discontinuities from SeaMARC II and three-dimensional magnetic studies, *J. Geophys. Res*. *97*, 6959–6982, doi:10.1029/91JB03065.

Carbotte, S. M., M. Marjanović, H. Carton, J. C. Mutter, J. P. Canales, M. R. Nedimović, S. Han, and M. R. Perfit (2013), Fine-scale segmentation of the crustal magma reservoir beneath the East Pacific Rise, *Nat. Geosci.*, *6*, 866–870, doi:10.1038/ngeo1933.

Chadwell, C. D., F. N. Spiess, J. A. Hildebrand, L. Prawirodirdjo, L. E. Young, G. H. Purcell, and H. Dragert (1995), The Juan de Fuca Ridge geodesy project: Strain and plate motion measurements using GPS and acoustics, *Eos Trans. AGU*, *76*, F412.

Chadwell, C. D., J. A. Hildebrand, F. N. Spiess, J. L. Morton, W. R. Normark, and C. A. Reiss (1999), No spreading across the Southern Juan de Fuca Ridge axial cleft during 1994–1996, *Geophys. Res. Lett.*, *26*, 2525–2528, doi:10.1029/1999GL900570.

Chadwick, W. W., Jr., and M. Stapp (2002), A deep-sea observatory experiment using acoustic extensometers: Precise horizontal distance measurements across a mid-ocean ridge, *IEEE J. Oceanic Eng.*, *27*, 193–201, doi:10.1109/JOE.2002.1002473.

Chadwick, W.W., Jr., R. W. Embley, H. B. Milburn, C. Meinig, and M. Stapp (1999), Evidence for deformation associated with the 1998 eruption of Axial Volcano, Juan de Fuca Ridge, from acoustic extensometer measurements, *Geophys. Res. Lett.*, *26*, 3441–3444.

Chadwick, W. W., Jr., S. L. Nooner, M. A. Zumberge, R. W. Embley, and C. G. Fox (2006), Vertical deformation monitoring at Axial Seamount since its 1998 eruption using deep-sea pressure sensors, *J. Volcanol. Geotherm. Res.*, *150*, 313–327, doi:10.1016/j.jvolgeores.2005.07.006.

Chadwick, W. W., Jr., S. L. Nooner, D. A. Butterfield, and M. D. Lilley (2012), Seafloor deformation and forecasts of the April 2011 eruption at Axial Seamount, *Nat. Geosci.*, *5*, 474–477, doi:10.1038/NGEO1464.

Chadwick, W.W., Jr., et al. (2013), The 1998 eruption of Axial Seamount: New Insights on submarine lava flow emplacement from high-resolution mapping, *Geochem. Geophys. Geosyst.*, *14*, 3939–3968, doi:10.1029/ggge. 20202.

Detrick, R. S., P. Buhl, E. Vera, J. Mutter, J. Orcutt, J. Madsen, and T. Brocher (1987), Multichannel seismic imaging of a crustal magma chamber along the East Pacific Rise, *Nature*, *326*, 35–41, doi:10.1038/326035a0.

Eble, M. C., F. I. Gonzalez, D. M. Mattens, and H. B. Milburn (1989), Instrumentation, field operations, and data processing for PMEL deep ocean bottom pressure measurements, *NOAA Tech. Memo. ERL PMEL-89*, 71 pp.

Einarsson, P. (1991), The Krafla rifting episode 1975–1989, in *Náttúra Mývatns (The Nature of Lake Mývatns)*, edited by A. Gardarsson, and Á. Einarsson, pp. 97–139, Iceland. Nat. Sci. Soc., Reykjavík, Iceland.

Fialko, Y., Y. Khazan, and M. Simons (2001), Deformation due to a pressurized horizontal circular crack in an elastic half-space, with applications to volcano geodesy, *Geophys. J. Int.*, *146*, 181–190, doi:10.1046/j.1365-246X.2001.00452.x.

Fofonoff, N. P., and R. C. Millard Jr. (1983), Algorithms for computation of fundamental properties of seawater, *UNESCO Tech. Pap. Mar. Sci.*, *44*, 53.

Fornari, D., et al. (2012), The East Pacific Rise between 9°N and 10°N: twenty-five years of integrated, multidisciplinary oceanic spreading center studies, *Oceanography*, *25*, 18–43, doi:10.5670/oceanog.2012.02.

Fox, C. G. (1990), Evidence of active ground deformation on the mid-ocean ridge: Axial Seamount, Juan de Fuca Ridge, April-June, 1988, *J. Geophys. Res.*, *95*, 12813–12822.

Fox, C. G. (1999), In situ ground deformation measurements from the summit of Axial Volcano during the 1998 volcanic episode, *Geophys. Res. Lett.*, *26*, 3437–3440.

Fujimoto, H., K. Koizumi, Y. Osada, and T. Kanazawa (1998), Development of instruments for seafloor geodesy, *Earth Planets Space*, *50*, 905–911.

Fujimoto, H., M. Mochizuki, K. Mitsuzawa, T. Tamaki, and T. Sato (2003), Ocean bottom pressure variations in the southeastern Pacific following the 1997-98 El Nino event, *Geophys. Res. Lett.*, *30*(9), 1456, doi:10.1029/2002GL016677, 9.

Fujita, M., M. Sato, T. Yabuki, M. Mochizuki, and A. Asada (2003), Examination on repeatability of GPS/Acoustic seafloor positioning for the reference points deployed around Japan, *Eos Trans. AGU 84*, Fall Meet. Abstract G21D-0297.

Gagnon, K., C. D. Chadwell, and E. Norabuena (2005), Measuring the onset of locking in the Peru–Chile trench with GPS and acoustic measurements, *Nature*, *434*, 205–208, doi:10.1038/nature03412.

Goss, A. R., M. R. Perfit, W. I. Ridley, K. H. Rubin, G. D. Kamenov, S. A. Soule, A. Fundis, and D. J. Fornari (2010), Geochemistry of lavas from the 2005–2006 eruption at the East Pacific Rise, 9°46′N-9°56′N: Implications for ridge crest plumbing and decadal changes in magma chamber compositions, *Geochem. Geophys. Geosyst.*, *11*, Q05T09, doi:10.1029/2009GC002977.

Gripp, A. E., and R. G. Gordon (2002), Young tracks of hotspots and current plate velocities. Geophysical Journal International, *Geophys. J. Int.*, *150*, 321–361, doi:10.1046/j.1365-246X.2002.01627.x.

Haymon, R. M., et al. (1993), Volcanic eruption of the mid-ocean ridge along the East Pacific Rise crest at 9°45–52′N: Direct submersible observations of seafloor phenomena associated with an eruption event in April, *1991. Earth Planet. Sci. Lett.*, *119*, 85–101, doi:10.1016/0012-821X(93)90008-W.

Ito, Y., T. Tsuji, Y. Osada, M. Kido, D. Inazu, Y. Hayashi, H. Tsushima, R. Hino, and H. Fujimoto (2011), Frontal wedge deformation near the source region of the 2011 Tohoku-Oki earthquake, *Geophys. Res. Lett.*, *38*, L00G05, doi:10.1029/2011GL048355.

Kent, G. M., A. J. Harding, and J. A. Orcutt (1993a), Distribution of magma beneath the East Pacific Rise between the Clipperton Transform and the 9°17′N Deval from forward modeling of common depth point data, *J. Geophys. Res.*, *98*, 13945–13696, doi:10.1029/93JB00705.

Kent, G. M., A. J. Harding, and J. A. Orcutt (1993b), Distribution of magma beneath the East Pacific Rise near the 9°03′N overlapping spreading center from forward modeling of common depth point data, *J. Geophys. Res.*, *98*, 13971–13995, doi:10.1029/93JB00706.

Luther, G., et al. (2012), Chemistry, temperature, and faunal distributions at diffuse-flow hydrothermal vents: Comparison of two geologically distinct ridge systems, *Oceanography 25*, 234–245, doi:10.5670/oceanog.2012.22.

Marjanović, M. (2013), *Signatures of present and past melt distribution along fast and intermediate spreading centers, PhD dissertation*, Columbia Univ., N. Y.

Marjanović, M., S. M. Carbotte, H. D. Carton, J. C. Mutter, M. R. Nedimović, and J. P. Canales (2013), Seismic images of multiple magma sills beneath the East Pacific Rise, Abstract OS42A-05 Presented at 2012 Fall Meet, AGU San Franc. Calif., 9–13 Dec.

McGuire, J. J., and J. A. Collins (2013), Millimeter-level precision in a seafloor geodesy experiment at the Discovery transform fault, East Pacific Rise, *Geochem. Geophys. Geosyst.*, *14*, 4392–4402, doi:10.1002/ggge.20225.

Mogi, K. (1958), Relations between the eruptions of various volcanoes and the deformation of the ground surfaces around them, *Bull. Earthquake Res. Inst. Univ. Tokyo 36*, 99–134.

Nagaya, Y., T. Urabe, and T. Yabuki (1999), Crustal deformation observation at the crest of the EPR 18.5S with the seafloor acoustic ranging method, *Eos Trans. AGU*, *80*(46), Fall Meet. Suppl. F1076.

Nooner, S.L. (2005), Gravity changes associated with underground injection of CO2 at the Sleipner storage reservoir in the North Sea, and other marine geodetic studies, Univ. of Calif., San Diego.

Nooner, S. L., and W. W. Chadwick (2009), Volcanic inflation measured in the caldera of axial seamount: Implications for magma supply and future eruptions, *Geochem. Geophys. Geosyst.*, *10*, Q02002, doi:10.1029/2008GC002315.

Nooner, S. L., O. Eiken, C. Hermanrud, G. S. Sasagawa, T. Stenvold, M. A. Zumberge (2007), Constraints on the in situ density of CO2 within the Utsira formation from time-lapse seafloor gravity measurements, *Int. J. Greenh. Gas Control*, *1*, 198–214, doi:10.1016/S1750-5836(07)00018-7.

Nooner, S. L., L. Bennati, E. Calais, W. R. Buck, I. J. Hamling, T. J. Wright, and E. Lewi (2009), Post-rifting relaxation in the Afar region, Ethiopia, *Geophys. Res. Lett.*, *36*, L21308, doi:10.1029/2009GL040502.

Osada, Y., H. Fujimoto, S. Miura, A. Sweeney, T. Kanazawa, S. Nakao, S. Sakai, J. A. Hildebrand, and C. D. Chadwell (2003), Estimation and correction for the effect of sound velocity variation on GPS/Acoustic seafloor positioning: An experiment off Hawaii Island. *Earth Planets Space*, *55*, e17–e20.

Polster, A., M. Fabian, and H. Villinger (2009), Effective resolution and drift of Paroscientific pressure sensors derived from long-term seafloor measurements, *Geochem. Geophys. Geosyst.*, *10*, Q08008, doi:10.1029/2009GC002532.

Rubin, K. H., J. D. Macdougall, and M. R. Perfit (1994), 210Po-210Pb dating of recent volcanic eruptions on the sea floor, *Nature*, *368*, 841–844, doi:10.1038/368841a0.

Sasagawa, G., W. Crawford, O. Eiken, S. Nooner, T. Stenvold, and M. Zumberge (2003), A new sea-floor gravimeter, *Geophysics*, *68*, 544–553.

Sato, M., T. Ishikawa, N. Ujihara, S. Yoshida, M. Fujita, M. Mochizuki, and A. Asada (2011), Displacement above the hypocenter of the 2011 Tohoku-Oki earthquake, *Science*, *332*, 1395–1395, doi:10.1126/science.1207401.

Shank, T. M., D. J. Fornari, K. L. Von Damm, M. D. Lilley, R. M. Haymon, and R. A. Lutz (1998), Temporal and spatial patterns of biological community development at nascent deep-sea hydrothermal vents (9°50′N, East Pacific Rise), *Deep Sea Res. Part II*, *45*, 465–515, doi:10.1016/S0967-0645(97)00089-1.

Soule, S. A., D. J. Fornari, M. R. Perfit, and K. H. Rubin (2007), New insights into mid-ocean ridge volcanic processes from the 2005–2006 eruption of the East Pacific Rise, 9°46′N–9°56′N, *Geology*, *35*, 1079–1082, doi:10.1130/G23924A.1.

Spiess, F. N., C. D. Chadwell, J. A. Hildebrand, L. E. Young, G. H. Purcell Jr., and H. Dragert (1998), Precise GPS/Acoustic positioning of seafloor reference points for tectonic studies, *Phys. Earth Planet. Inter.*, *108*, 102–112.

Stenvold, T., O. Eiken, M. A. Zumberge, G. S. Sasagawa, and S. L. Nooner (2006), High-precision relative depth and subsidence mapping from seafloor water-pressure measurements, *SPE J.*, *11*, 380–389.

Tolstoy, M., S. Constable, J. Orcutt, H. Staudigel, F. K. Wyatt, and G. Anderson (1998), Short and long baseline tiltmeter measurements on axial seamount, Juan de Fuca Ridge, *Phys. Earth Planet. Inter.*, *108*, 129–141, doi:10.1016/S0031-9201(98)00091-0.

Tolstoy, M., et al. (2006), A sea-floor spreading event captured by seismometers, *Science*, *314*, 1920–1922, doi:10.1126/science.1133950.

Tryggvason, E. (1984), Widening of the Krafla fissure swarm during the 1975–1981 volcano-tectonic episode, *Bull. Volcanol.*, *47*, 47–69, doi:10.1007/BF01960540.

Vera, E. E., J. C. Mutter, P. Buhl, J. A. Orcutt, A. J. Harding, M. E. Kappus, R. S. Detrick, and T. M. Brocher (1990), The Structure of 0- to 0.2-m.y.-Old Oceanic Crust at 9° N on the East Pacific Rise From Expanded Spread Profiles, *J. Geophys. Res.*, *95*, 15,529–15,556.

Von Damm, K. L. (2004), Evolution of the hydrothermal system at East Pacific Rise 9°50′N: Geochemical evidence for changes in the upper oceanic crust, in *Geophysical Monograph Series*, edited by C. R. German, J. Lin, and L. M. Parson, pp. 285–304, AGU, Washington, D. C.

Waldhauser, F., and M. Tolstoy (2011), Seismogenic structure and processes associated with magma inflation and hydrothermal circulation beneath the East Pacific Rise at 9°50′N, *Geochem. Geophys. Geosyst.*, *12*, Q08T10, doi:10.1029/2011GC003568.

Watanabe, T., H. Matsumoto, H. Sugioka, H. Mikada, and K. Suyehiro (2004), Offshore monitoring system records recent earthquake off Japan's Northernmost island, *Eos Trans. AGU*, *85*, 14.

Watts, D.R., and H. Kontoyiannis (1990), Deep-ocean bottom pressure measurements, *J. Atmos. Oceanic Technol.*, *7*, 296–306.

West, M. E., W. Menke, M. Tolstoy, S. Webb, and R. Sohn (2001), Magma storage beneath Axial Volcano on the Juan de Fuca mid-ocean ridge, *Nature*, *413*, 833–836.

White, S.M., R. M. Haymon, and S. Carbotte (2006), A new view of ridge segmentation and near-axis volcanism at the East Pacific Rise, 8°-12°N, from EM300 multibeam bathymetry, *Geochem. Geophys. Geosyst.*, *7*, Q12O05, doi:10.1029/2006GC001407.

Wright, T. J., et al. (2012), Geophysical constraints on the dynamics of spreading centres from rifting episodes on land, *Nat. Geosci.*, *5*, 242–250, doi:10.1038/ngeo1428.

Yücel, M., and G. W. Luther (2013), Temporal trends in vent fluid iron and sulfide chemistry following the 2005/2006 eruption at East Pacific Rise, 9°50′N: Fe-S, *Geochem. Geophys. Geosyst.*, *14*, 759–765, doi:10.1002/ggge.20088.